Publ. Astron. Obs. Belgrade No. 104 (2024), 19 - 28 *Invited Review*
https://doi.org/10.69646/aob104p019

SUPERNOVAE AS TRACERS OF THE STRUCTURE AND EVOLUTION OF THE SURROUNDING UNIVERSE

PETR KURFÜRST

Department of Theoretical Physics and Astrophysics, Faculty of Science, Masaryk University, Kotlářská 2, 61137 Brno, Czech Republic
E–mail: petrk@physics.muni.cz

Abstract. The impact of mass lost from hot stars in general, including supernovae (SNe), as probably the leading contributor, has a direct impact on the evolution not only of stars but the entire universe. We study the interactions of expanding supernova (SN) envelopes with aspherical dense circumstellar medium (CSM) of various morphologies, including circumstellar disks, bipolar lobes, or overdense layers of colliding ejected matter in binary systems. Many possible mechanisms can lead to wild eruptions of vast amounts of matter from potential SNe progenitors for a long time or shortly before the SN explosion. These effects are manifested by irregularities and bumps in light curves and asymmetries in spectra. Since massive stars usually end their lives as SNe, they appear to be candidates for neutron stars, black holes, gamma-ray bursts, or magnetars; understanding the behavior of the processes shortly before and after the SN explosions and their impact on the surroundings will help us understand how the stars become precursors to these exotic and interesting stellar objects.

1. INTRODUCTION

How important is the role of supernovae (SNe) that strongly interact with pre-existing circumstellar material in related astrophysical processes? In this context, the main objective of our research was to create hydrodynamic models of interactions of expanding SNe with different morphologies of a surrounding circumstellar material (CSM) and study their implications for observations. We also describe the possible use of the original Czech satellite QUVIK, which was designed mainly for ultraviolet (UV) observations of kilonovae (KNe; merging of neutron stars), but observations of other types of astrophysical transients such as SNe, gamma-ray bursts (GRBs) and others are also expected. We expect that SNe interactions with CSM provide critical clues about massive stars and their mass loss, providing a unique "tool" for revealing the progenitor's mass-loss history. Complex studies (theoretical and observational) of these events can be used to probe CSM density distribution and constrain various proposed theories of the final fate of massive stars.

The SN phenomenon may occur during the final stages of massive ($M_{\rm init} \geq 8\,M_{\odot}$) stars; the main supernova types and their progenitors are illustrated in Fig. 1. They are considered the universe's factories that synthesize and spread new elements (including those heavier than iron) into space. The kinetic energy and momentum of the explosion can significantly influence star formation, which affects the evolution of entire galaxies on a global scale. The last observations of the James Webb space telescope significantly enhanced the role of massive stars as dust producers (e.g., Agliozzo et al. 2021), contributing thus to the formation of planets (and ultimately

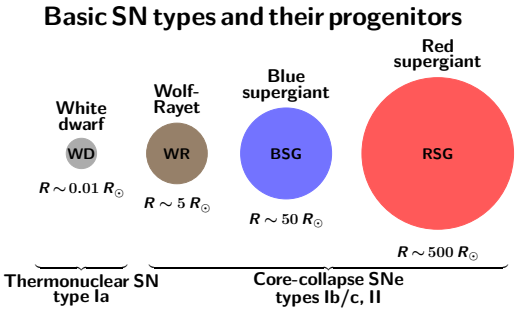

Figure 1: Inspired by Ehud Nakar's talk on 35HUJI - Jerusalem Winter School on Transients 2017/2018.

to the emergence of life). Massive SNe leave behind compact objects such as neutron stars (NS) or black holes (BH). The NS or BH binaries can merge with an associated burst of gravitational wave emission, as was observed by LIGO and VIRGO detectors (e.g., Abbott et al. 2016, 2017). SNe can be used for precise inferences of distances in the universe, which led to the concept of dark energy supported by the discovery of accelerating expansion of the universe (e.g., Perlmutter et al. 1999).

2. INTERACTIONS OF SNE WITH CSM

2. 1. PRE-SN MASS LOSS

The evolution of massive stars is governed by huge amounts of mass expelled from their surfaces. Many massive stars undergo episodic mass ejections, losing several $M_\odot$ (or more) over several dynamical timescales. A typical example is η Car, which ejected $10-20\,M_\odot$ during its 19th century eruption (e.g., Smith 2006). Such eruptions may occur just a few years before the final SN explosion (e.g., Ofek et al. 2014). According to the reduction of main sequence (MS) stars' winds mass loss due to the clumping (Šurlan et al. 2012), the dominant "burden" of mass loss has shifted to post-MS stars' (mainly supergiants') winds and eruptions, as well as binary mass transfer. Dramatic confirmations of such eruptive mass ejections provide the Type IIn (narrow lines) SNe, which are enveloped in huge clouds of material ejected only a few years before core collapse. These eruptions likely indicate severe instabilities in the final stages of nuclear burning. Figure 2 shows a basic overview of the mass-loss rates of stellar winds and eruptions from different types of stars (see also Heger et al. 1997, Fuller 2017). Roche lobe overflow (RLOF) in binaries can also result in intense mass transfer and accretion (Kashi & Soker 2010), or the binary can experience a common envelope phase or even a merger (Podsiadlowski et al. 1992; Smith 2011). These structures are observed around massive stars and can be revealed by two/or multi-component line profiles in SN spectra (Andrews et al. 2017), peak multiplicity in nebular SN spectra (Andrews & Smith 2018a), spectropolarimetry (Patat et al. 2011), or by combining these (Bilinski et al. 2018). Studying SNe properties in a wide range of situations is thus essential to understanding the evolution and final fate of massive stars and their surroundings.

2. 2. STRONGLY INTERACTING SNE

After an SN explosion, the expanding blast wave shocks and sweeps up the surrounding material, potentially leaving imprints in light curves and spectra. In some SNe,

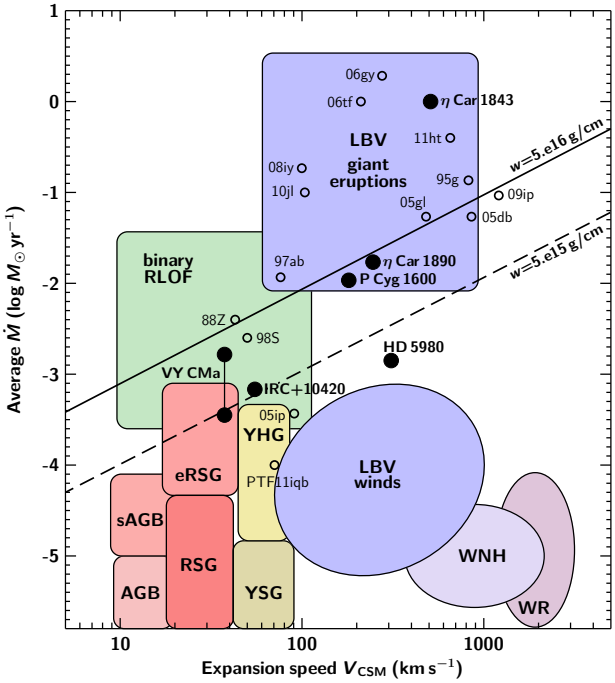

Figure 2: Mass-loss rate $\dot{M}$ as a function of wind velocity, comparing values for interacting SNe to those of known types of stars. The two diagonal lines indicate the value for a moderate-luminosity SN IIn, and a typical lower bound for wind densities required to make a SN IIn (dashed line). Adapted from Smith (2017).

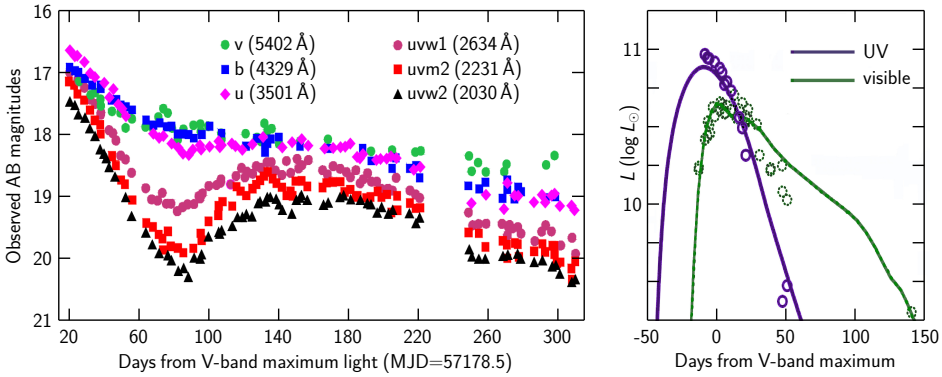

Figure 3: Multiwavelength graphs of late-time SN emission. *Left*: UVOT light curves of ASASSN-15lh (adapted from Brown et al. 2016). *Right*: UV and V-band light curves of SLSN I Gaia16apd (adapted from Tolstov et al. 2017)

the interaction with the CSM significantly dominates the observable characteristics of "standard" SNe, providing a unique "tool" for revealing the mass-loss history (e.g., Woosley et al. 2007; Smith 2017). Figure 3 demonstrates the characteristic light curve of a typical SLSN that shows rebrightening in a particular phase and very long duration; it also compares the UV and visible bands in the early phase. The

SN-CSM collision is very efficient in converting ejecta kinetic energy to radiation, and the interacting SN can be much more luminous than "ordinary" SN. The typical observational manifestations of this process are the narrow emission lines produced within the photo-ionized CSM; the SN is then classified as IIn (if hydrogen-rich) or Ibn (if hydrogen-poor). Such SNe comprise about 10% of all core-collapse SNe (e.g., Smith 2011). Multi-wavelength photometry and spectroscopy of these events can probe CSM's density distribution.

Aspherical CSM collisions can lead to qualitatively different effects than spherically symmetric ones. For example, the SN ejecta can envelop and "swallow" the shock, thus hiding interaction signatures such as narrow emission lines (Smith 2017). The SN can then behave like an additional power source deep in the ejecta. The significance of such effects in powering IIn-P (plateau) SNe and peculiar objects like SN iPTF14hls has been recognized by, e.g., Arcavi (2017) and Andrews & Smith (2018b). Not many theoretical works on the observational characteristics of interacting SNe have gone beyond spherical symmetry; still less exploring the observables from different viewing angles. van Marle et al. (2010) performed 2D hydrodynamics of a spherical SN collision with an asymmetric bipolar nebula (resembling η Car) and a dense shell added on top of a spherical wind; they calculated light curves with optically thin cooling assumptions. Vlasis et al. (2016) performed M1 multigroup 2D radiative hydrodynamics (RHD) of a spherical SN impinging on oblate and prolate ellipsoidal CSM distributions with varying axis ratios, a spherical CSM hit by an oblate or prolate SN ejecta, and a spherical SN colliding with a disk. McDowell et al. (2018) performed hydrodynamic (HD) calculations of an SN-disk interaction. They estimated the light curves by combining numerical shock heating rates with a simple one-zone model of the SN light curve. The interactions of the SN with various morphologies of aspherical CSM, including the calculation of light curves, spectra, and polarization, were recently studied by Kurfürst et al. (2020), and the work continues as one of the main research topics within our team strategy.

3. COMPUTATIONAL SETUP

In our models, we include three components of CSM: initially spherically symmetric SN ejecta, spherically symmetric stellar wind, and various types and morphologies of aspherical CSM. We describe here an example of the initial state of the SN interaction with the dense equatorial disk: the density $\rho_{\rm wind}$ of the surrounding isotropic stellar wind is set to $\propto r^{-2}$ where r is the spherical radial distance from the origin of coordinates (progenitor center). Density profile of the equatorial disk $\rho_{\rm disk}$ is set to

$$\rho_{\rm disk} \propto r^{-2}\, {\rm e}^{-\frac{z^2}{2{\rm H}^2}}, \tag{1}$$

where z is the vertical coordinate, and H is the disk scaleheight, $H = a/\Omega$ with a being the sound speed as a function of the initially decreasing temperature $T \sim r^{-0.35}$, and $\Omega = \sqrt{GM_\star/r^3}$ is the disk (Keplerian) angular velocity (cf. Kurfürst et al. 2014, 2018, Kurfürst & Krtička 2019). Density profiles of all other types of aspherical CSM are more complicated; for this reason, they had to be pre-calculated numerically and mapped onto the computational code grid. The boundary conditions were set as inflow at the inner boundary, outflow at the outer boundary, and reflecting at the latitudinal ones. Calculation of shock heating rate $\dot{q}$ within the HD simulations is

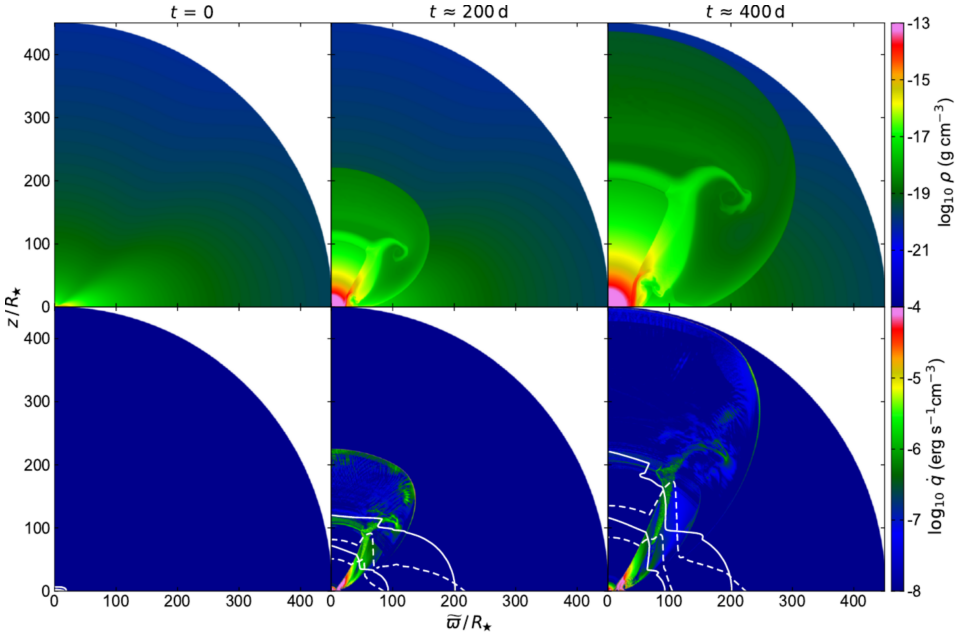

Figure 4: Stages in the evolution of the density ρ and the shock heating rate $\dot{q}$ within SN ejecta interacting with dense circumstellar disk (model A) produced by, e.g., the intense binary RLOF. The white lines denote the calculated edges of the optical depth τ values 0.1 and 1, seen either from the polar or equatorial direction. 2D model, adapted from Kurfürst et al. 2020.

performed via

$$\dot{q} = \int \frac{\mathrm{d}}{\mathrm{dt}} \frac{P - P_{\mathrm{isen}}}{\gamma - 1} \,\mathrm{d}V, \quad \rho^{-\gamma} P_{\mathrm{isen}} = \mathrm{const.}, \tag{2}$$

where P is the pressure calculated directly from the model while P_{isen} is the isentropic pressure calculated as a passive scalar (Kurfürst et al. 2020, cf. also McDowell et al. 2018) and γ is the adiabatic index.

For the numerical calculations, we used our own Eulerian, multidimensional (2D, currently also 3D) magneto-hydrodynamic code with implemented flux-diffusion approximation and radiative cooling $\Delta F \propto \rho^2 \Lambda$ (where F is the energy flux, ρ is the density, and Λ is the tabulated cooling function). The radiative cooling $\sim \rho^2$ increases its efficiency in later phases of enhanced nebulosity of the ejecta; this leads to the creation of stronger instabilities and inhomogeneities in the CSM "soup" which further affects the radiative properties of the interacting zone. As a more advanced step, we recently calculated the bolometric light curves also using the radiation transfer (RT) Monte Carlo (MC) code SEDONA (Kasen et al. 2007, Kurfürst et al., in prep.).

We calculate shock propagation through a realistic progenitor (nonrotating red supergiant with the mass of $15\,M_\odot$ and radius $1000\,R_\odot$) using 1D RHD code SNEC (*Supernova Explosion Code*, Morozova et al. 2015). The internal shock propagating up to the stellar surface calculated by SNEC is at the moment of shock breakout remapped onto our 3D RHD Eulerian code, using 6000 radial, 480 polar (within one polar quadrant, and 72 azimuthal grid cells (Kurfürst et al., in prep.)

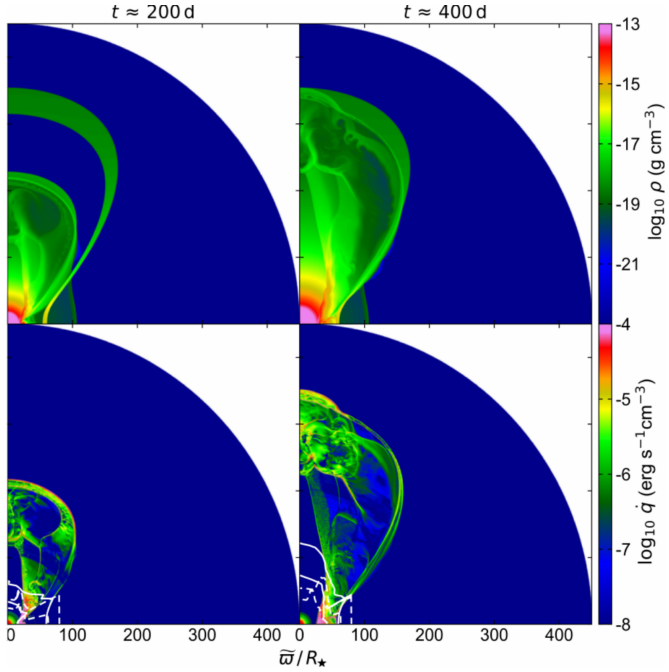

Figure 5: As in Figure 4, now for the bipolar lobes structure that mimics the configuration similar to the famous Homunculus Nebula surrounding the star η Car (model C). 2D model, adapted from Kurfürst et al. 2020.

4. HYDRODYNAMICAL AND RADIATIVE MODELS

We performed high-resolution, spherical SN hydrodynamical simulations interacting with several types and morphologies of possible circumstellar asymmetric environments, such as circumstellar disks (model A), bipolar lobes (model C), and various configurations of colliding winds (CW) shell structures (models B; see Figures 4 and 5). We aimed to discern observable features that would allow us to distinguish different CSM geometries from the underlying observable SNe. Since many aspherical CSM distributions are associated with different aspects of binary evolution, constraints on CSM geometry can probe the binary configuration. In particular, we study the hydrodynamical interaction of SN outflows with colliding binary wind envelopes for the first time. We aimed to shed light on the qualitative differences between different CSM geometries; we have not yet addressed such interactions for specific SN events.

Using this, we calculated the observable features of such interactions, namely the bolometric light curves and the line-of-sight velocity distributions in the nebular phase of the SN expansion from different viewing angle observational directions, which may be considered prototypes of the spectra (demonstrated in Figures 6 and 7). We also estimated the polarization degree of the SN ejecta using the analytical prescriptions of Brown & McLean (1977), including Thomson scattering in an optically thin centrally irradiated envelope. These approximations allow us to get at least a relative assessment of the asphericity induced by the different CSM geometries.

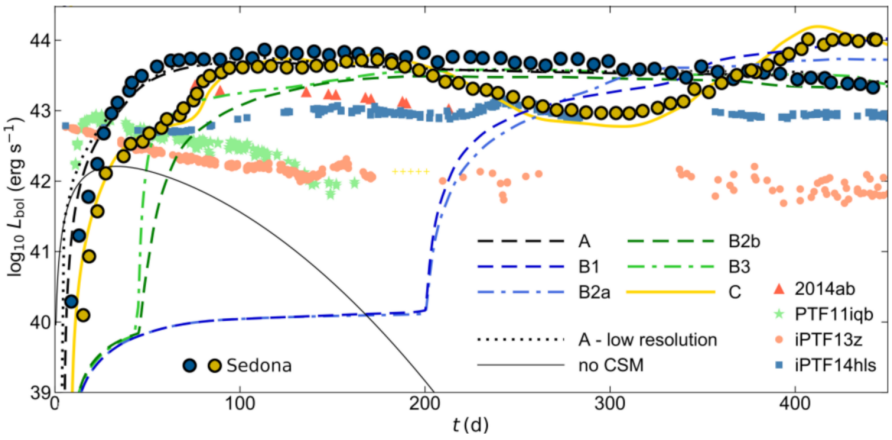

Figure 6: Bolometric light curves of our models either by Arnett's law (Arnett 1982) or 3D Monte Carlo (MC) radiation transfer (RT) code Sedona (see Kasen et al. 2007, current 3D calculations in Kurfürst et al., in prep.) in models A-disk and C-lobes (models B are various configurations of CW shells). The thin black solid line labeled "no CSM" corresponds to a hypothetical SN without CSM interaction but radioactively heated. The light curves are compared with the denoted observed SNe (cf. Kurfürst et al. 2020).

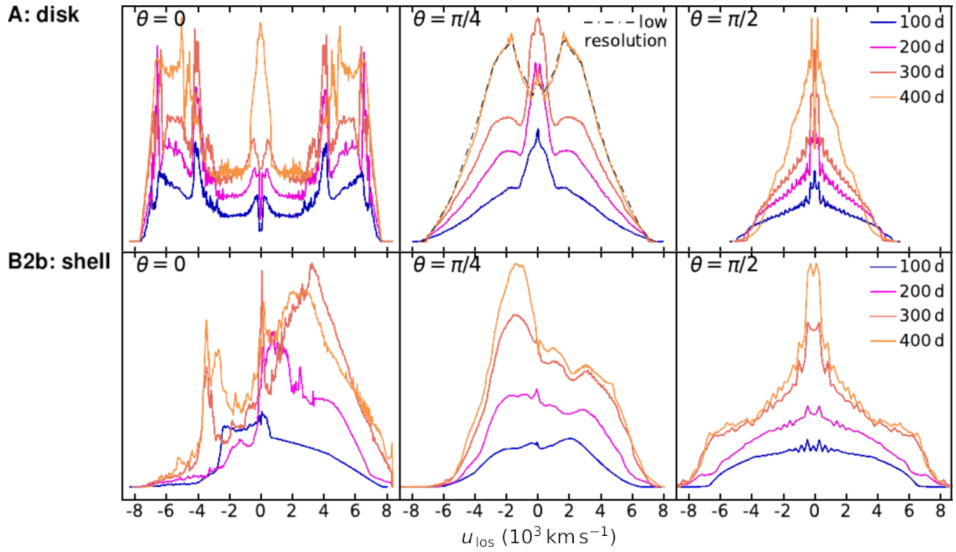

Figure 7: Line-of-sight velocity distributions (proxy-spectra, calculated only from the outer "nebulous" part of SN envelope and excising the inner still dense part corresponding to helium core of the star) for different models, labeled on the left. Each column represents a different viewing angle θ. Colored lines are results for different simulation times with legend given in the plot. Adapted from Kurfürst et al. 2020.

In the subsequent study, we calculated the SNe interactions of colliding winds in binaries using the 3D RHD code RAMSES (Pejcha et al. 2022); we performed in this work different types of simulations, including adiabatic colliding winds and radiatively efficiently cooled colliding winds. We studied such interactions for two identical stars (equal stellar winds) and unequal wind strengths. As a result, we found from those RHD simulations that such CW structures are likely disfavoured for most situations produced by stationary stellar winds because the luminosity induced by shock power $\dot{q}$ would exceed the typical type IIP SN luminosity only in case of double red supergiant binaries with the mass ratio of the two components $q \geq 0.9$, with the stellar wind mass-loss rates $\dot{M} \geq 10^{-4}\, M_{\odot}\, \mathrm{yr}^{-1}$, and with the relative orbital distance $a \sim 50 - 1500\,\mathrm{AU}$ which is too rare. In any case, even these interactions cannot be completely ruled out, especially if we consider that the overdense shells of colliding winds can be produced not only by standard stationary winds but also by various combinations of violent eruptive events in the final stages of binary evolution.

5. MONITORING OF TRANSIENTS BY CZECH SATELLITE QUVIK

One of the most significant advances in physics in recent years is the detection of gravitational waves by the Laser Interferometer Gravitational-Wave Observatories (LIGO) and Virgo. The detection of the short gamma-ray burst GRB170817 as a product of the merger of two closely orbiting neutron stars, which was successfully identified with the gravitational wave source GW170817, represents a milestone in multi-messenger astrophysics. Modern space observatories observing many types of astronomical transients, such as SNe, GRBs, and others, have grown into large and very costly missions. Our group is involved in the nanosatellite HERMES-SP project and the CAMELOT initiative, including two in-orbit demonstration missions, GRBAlpha and VZLUSAT-2. One of these nanosatellites, GRBAlpha, has been successfully operating in orbit since March 2021 and has detected a number of gamma-ray bursts. VZLUSAT-2 successfully launched in January 2022 and has detected several gamma-ray bursts and solar flares. Our research group is leading the data analysis and scientific use of the GRB detectors on these missions.

Our research group has initiated the project of the QUVIK (Quick Ultraviolet Survey of Kilonovae) space UV telescope, with a mass of $\sim 80\,\mathrm{kg}$ and a moderately fast object acquisition capability ($\sim 15\,\mathrm{min}$) and a near real-time alert communication system. The mission, which has recently been approved and selected for funding by the Czech Ministry of Transport, will perform photometry of kilonovae produced by neutron star mergers in both the near and far UV bands and thus be able to discriminate between different scenarios of these events. Other main objectives (except kilonovae) will include GRBs, SNe, hot stars, galactic nuclei, tidal disruption events, neutron stars, fast radio bursts, etc (Werner et al. 2023, Krtička et al. 2023, Zajaček et al. 2023). In the case of SNe, the satellite will measure the UV flux in the early phase, right after the shock breakout (after the Israeli ULTRASAT satellite alerts), and also in late phases in case of bumps and rebrightenings caused by strong SN-CSM interactions. Specification of the satellite: mass approx. 130 kg, altitude approx. 550 km, dims approx. 0.7×0.7×1.1m, FUV range: 1400 - 1900 Å, NUV range: 2600 - 3600 Å, resolution (FWHM) ≤ 2.5 arcsecond, sensitivity ∼22 AB mag, slew time ∼15 min, complementarity to ULTRASAT. sensitivity 22 AB mag. The project is led by the Czech Aerospace Research Centre (VZLU), which is also responsible for all

the technical design of this mission. Our research group and the wider community of mainly Czech astrophysicists are leading the scientific preparation, including selecting the science objectives and requirements. The mission is scheduled to launch in 2028 and is expected to last about 5 years.

6. SUMMARY

Observations of SNe have revealed a puzzling diversity of CSM surrounding the progenitor star at distances of tens to thousands of AU; the likely most significant reason for the formation of such a dense CSM that the exploding SN will manifest as IIn or SLSN is that many massive stars lose substantial amounts of mass shortly before their core collapses. Moreover, spectral line profiles and (spectro)polarimetry suggest that the CSM around many SNe lacks spherical symmetry. Using our HD models and RT SEDONA calculations, we estimated three observables of SN-CSM interaction in various CSM morphologies: $L_{\rm bol}$, distribution of $V_{\rm los}$ as a proxy for late-time (nebular) spectral line profiles, and the degree of polarization. Colliding wind shells are located only on one side of the SN; they could be an attractive possibility for explaining the CSM overdensities and the blue-red asymmetry of line profiles at late times. However, detailed 3D RHD simulations of CW radiative shells disfavor the colliding stationary winds' produced structures: We estimate that $\ll 1\,\%$ of all collapsing massive stars satisfy the conditions on binary mass ratio and separation to form so thick and dense CW shells that could produce a significant shock radiative efficiency.

Regarding our future work: Connecting the 3D RHD and RT models with observations, we aim to determine more precisely the structures of the surrounding CSM to understand better the quantity and morphology of the mass loss of post-MS massive stars beyond the standard predictions for stellar winds. Among even more ambitious aims is to illuminate the final phases of massive star evolution, leading up to the SN explosions and other types of extremely energetic transients. To understand and correctly interpret observed data of massive stars and SNe, developing sophisticated multidimensional methods and codes that account for different physical effects and geometries is necessary for success in nearly every astronomical and astrophysical research approach, as large surveys and high-resolution simulations become the norm. Regarding the QUVIK collaboration, we expect that UV photometry will contribute significantly to our understanding of the non-stationary, eruptive pre-explosive ejections, and enhanced mass loss of stars.

Acknowledgements

This work was supported by grant 31 2217 - GAČR GF23-04053L. Computational resources were supplied by the project "e-Infrastruktura CZ" (e-INFRA LM2018140) provided within the program Projects of Large Research, Development and Innovations Infrastructures.

References

Abbott, B. P., Abbott, R., Abbott, T. D., Abernathy, M. R., Acernese, F., Ackley, K., Adams, C., Adams, T., and others: 2016, *Physical Review Letters*, **116**, 13.

Abbott, B. P., Abbott, R., Abbott, T. D., Acernese, F., Ackley, K., Adams, C., Adams, T., and others: 2017, *Physical Review Letters*, **118**, 22.

Agliozzo, C., Phillips, N., Mehner, A., Baade, D., Scicluna, P., Kemper, F., Asmus, D., de Wit, W. J., Pignata, G.: 2021, *The Astrophysical Journal*, **655**, A98.

Andrews, J. E., Smith, N., McCully, C., Fox, O. D., Valenti, S., Howell, D. A.: 2017, *Monthly Notices of the Royal Astronomical Society*, **471**, 4.
Andrews, J. E., Smith, N.: 2018, *Monthly Notices of the Royal Astronomical Society*, **477**, 74.
Arcavi, I.: 2017, *What Type of Star Made the One-of-a-kind Supernova iPTF14hls?*, HST Proposal id.15222.
Arnett, W. D.: 1982, *The Astrophysical Journal*, **253**, 785.
Bilinski, C., Smith, N., Williams, G., Smith, P., Zheng, W., Graham, M. L., Mauerhan, J. C., and others: 2018, *Monthly Notices of the Royal Astronomical Society*, **475**, 1.
Brown, J. C., McLean, I. S.: 1977, *Astronomy and Astrophysics*, **57**, 141.
Brown, P. J., Yang, Y., Cooke, J., Olaes, M., Quimby, R. M., Baade, D., Gehrels, N., and others: 2016, *The Astrophysical Journal*, **828**, 1.
Fuller, J.: 2017, *Monthly Notices of the Royal Astronomical Society*, **470**, 2.
Heger, A., Jeannin, L., Langer, N., Baraffe, I.: 1997, *Astronomy and Astrophysics*, **327**, 224.
Kasen, D., Woosley, S., Nugent, P., Röpke, F.: 2007, *Journal of Physics Conference Series*, **78**, 012037.
Kashi, A., Soker, N.: 2010, *The Astrophysical Journal*, **723**, 1.
Krtička, J., Benáček, J., Budaj, J., Korčáková, D., Pál, A., Piecka, M., Zejda, M., Bakış, V., Brož, and others: 2023, *arXiv e-prints*, arXiv:2306.15081
Kurfürst, P., Feldmeier, A., Krtička, J.: 2014, *Astronomy and Astrophysics*, **569**, A23.
Kurfürst, P., Feldmeier, A., Krtička, J.: 2018, *Astronomy and Astrophysics*, **613**, A75.
Kurfürst, P., Krtička, J.: 2019, *Astronomy and Astrophysics*, **625**, A24.
Kurfürst P., Pejcha, O., Krtička, J.: 2020, *Astronomy and Astrophysics*, **642**, A214.
McDowell, A. T.,Duffell, P. C., Kasen, D.: 2018, *The Astrophysical Journal*, **856**, 1.
Morozova, V., Piro, A. L., Renzo, M., Ott, C. D., Clausen, D., Couch, S. M., Ellis, J., Roberts, L. F.: 2015, *The Astrophysical Journal*, **814**, 63.
Ofek, E. O., Sullivan, M., Shaviv, N. J., Steinbok, A., Arcavi, I., Gal-Yam, A., and others: 2014, *The Astrophysical Journal*, **789**, 2.
Patat, F., Taubenberger, S., Benetti, S., Pastorello, A., Harutyunyan, A.: 2011, *Astronomy and Astrophysics*, **527**, L6.
Pejcha, O., Calderón, D., Kurfürst, P.: 2022, *Monthly Notices of the Royal Astronomical Society*, **510**, 3.
Perlmutter, S., Aldering, G., Goldhaber, G., Knop, R. A., Nugent, P., Castro, P. G., and others: 1999, *The Astrophysical Journal*, **517**, 2.
Podsiadlowski, P., Joss, P. C., Hsu, J. J. L.: 1992, *The Astrophysical Journal*, **391**, 246.
Smith, N.: 2006, *The Astrophysical Journal*, **367**, 2.
Smith, N.: 2011, *Monthly Notices of the Royal Astronomical Society*, **415**, 3.
Smith, N.: 2017, *Handbook of Supernovae*, 403.
Šurlan, B., Hamann, W. R., Kubát, J., Oskinova, L. M., Feldmeier, A.: 2012, *Astronomy and Astrophysics*, **541**, A37.
Tolstov, A., Zhiglo, A., Nomoto, K., Sorokina, E., Kozyreva, A., Blinnikov, S.: 2017, *The Astrophysical Journal Letters*, **845**, 1.
van Marle, A. J., Smith, N., Owocki, S. P., van Veelen, B.: 2010, *Monthly Notices of the Royal Astronomical Society*, **407**, 4.
Vlasis, A., Dessart, L., Audit, E.: 2016, *Monthly Notices of the Royal Astronomical Society*, **458**, 2.
Werner, N., Řípa, J., Thöne, C.. Münz, F., Kurfürst, P., and others: 2023, *arXiv e-prints*, arXiv:2306.15080.
Woosley, S. E., Blinnikov, S., Heger, A.: 2007, *Nature*, **450**, 390.
Zajaček, M., Czerny, B., Jaiswal, V. K., Štolc, M., Karas, V., Pasham, D. R., Śniegowska, M., Witzany, V., Suková, P., Münz, F., Werner, N., Řípa, J., Labaj, M., Kurfürst, P., and others: 2023, *arXiv e-prints*, arXiv:2306.15082.